On the basis of these results, it is likely that there has been a significant human influence on the observed North American warming in the second half of the 20th century, associated with increasing atmospheric concentrations of greenhouse gases and sulfate aerosols. Over the 20th century, this influence is manifest not only in mean temperature changes but also in changes of the north-south temperature gradient, the temperature contrast between land and ocean, and reduction of the diurnal temperature range.

References and Notes

1. J. T. Houghton *et al*., Eds., *Climate Change 2001: The Scientific Basis* (Cambridge Univ. Press, Cambridge, 2001).
2. K. Braganza *et al*., *Clim. Dyn.* **20**, 491 (2003).
3. J. F. B. Mitchell *et al*., in *Climate Change 2001: The Scientific Basis*, J. T. Houghton *et al*., Eds. (Cambridge Univ. Press, Cambridge, 2001), pp. 695–738.
4. P. A. Stott, S. F. B. Tett, *J. Clim.* **11**, 3282 (1998).
5. F. W. Zwiers, X. Zhang, *J. Clim.* **16**, 793 (2003).
6. P. A. Stott, *Geophys. Res. Lett.* **30**, 1728 (2003).
7. T. R. Karl, R. W. Knight, D. R. Easterling, R. G. Quayle, *Bull. Am. Meteorol. Soc.* **77**, 279 (1996).
8. P. D. Jones, M. New, D. E. Parker, S. Martin, I. G. Rigor, *Rev. Geophys.* **37**, 173 (1999).
9. M. New, M. Hulme, P. D. Jones, *J. Clim.* **13**, 2217 (2000), updated by T. Mitchell at the Climatic Research Unit, University of East Anglia.
10. We applied a low-pass, 21-point binomial filter (half power at periods near 10 years), as used in the Intergovernmental Panel on Climate Change (IPCC) assessment (*1*).
11. A brief description of the five climate models is provided in the Supporting Online Material, together with references to publications providing more details.
12. For each of the models, we used data from long control simulations that have been performed with no changes to the external forcing parameters. The control simulations include 990 years of data from HadCM2, 1830 years from HadCM3, 500 years from GFDL R30, 240 years from ECHAM4, and 530 years from NCAR PCM. The 530-year period from PCM came from years 390 to 919 of the control run, after most of the initial climate drift had stabilized. Data for DTR were not available from the HadCM3 model and could not be determined from the GFDL model, which does not include a diurnal cycle of solar irradiance.
13. The anthropogenically forced model simulations include anthropogenic changes in well-mixed greenhouse gases, ozone (for some of the models), and sulfate aerosols. The major changes in radiative forcing are due to the changes in greenhouse gases and sulfate aerosols, so these are described as GS simulations. For the GFDL and HadCM2 models, these changes are expressed as an increase in equivalent CO_2 according to IPCC scenario IS92a for the period 1880–2000, along with estimated observed changes in anthropogenic sulfate aerosols represented through regional changes to surface albedo. For the HadCM3 (*21*), ECHAM4, and PCM (*22*) models, observed increases in individual major anthropogenic greenhouse gases are included, together with changes in tropospheric and stratospheric ozone and an explicit treatment of the direct radiative effect of sulfate aerosols. HadCM3 and ECHAM4 also include parameterizations for indirect sulfate forcing effects via cloud albedo changes. From HadCM2 and HadCM3, we have four independent members of an ensemble of simulations with different initial conditions, three GS ensemble members from GFDL R30, two from ECHAM4, and seven from PCM.
14. The natural externally forced model simulations include fixed greenhouse gas concentrations and estimated changes in total solar irradiance and stratospheric volcanic aerosol optical depth for the period 1880–1999. Somewhat different solar and volcanic forcing data sets are used for the different models. For the HadCM2 (three ensemble members) and HadCM3 (four ensemble members) simulations, the solar forcing is based on Lean *et al*. (*23*) and the volcanic forcing is based on updated data from Sato (*24*). For the GFDL model (*20*), the solar forcing is based on Lean (*25*) and the volcanic forcing is based on Andronova *et al*. (*26*). For the NCAR PCM simulations (*27*) (four ensemble members), the solar forcing is based on Hoyt and Schatten (*28*) and the volcanic forcing is based on Ammann *et al*. (*29*). For the GFDL model, simulations with natural external forcing alone were not available, so the NAT response was estimated from the difference between model simulations with all forcings (both anthropogenic forcing and natural external forcing, three ensemble members each) and simulations with anthropogenic forcing alone (three ensemble members); that is, NAT response ~ (GS + NAT) response – GS response. For the HadCM2 model, only simulations with separate solar (SOL) and volcanic (VOL) forcing were available, so the NAT response was estimated as the sum of these model responses; that is, NAT response ~ SOL response + VOL response.
15. J. Bell, P. B. Duffy, C. Covey, L. Sloan, *Geophys. Res. Lett.* **27**, 261 (2001).
16. The uncertainty of the ensemble mean 50-year and 100-year trends due to natural internal variability was estimated by resampling trends from the long control simulations from the respective models and allowing for the number of members in each ensemble. Further details of the approach used for estimating natural internal variability are given in the Supporting Online Material.
17. Consistency here means that the observed trend lies within the 90% confidence interval for the ensemble-mean forced trend (shown as the error bar about the forced model trend) combined with the 90% confidence interval for a single realization due to natural internal climate variability (shown as the error bar about zero trend).
18. S. F. B. Tett, P. A. Stott, M. R. Allen, W. J. Ingram, J. F. B. Mitchell, *Nature* **399**, 569 (1999).
19. P. A. Stott, S. F. B. Tett, M. R. Allen, J. F. B. Mitchell, G. J. Jenkins, *Science* **290**, 2133 (2000).
20. A. J. Broccoli *et al*., in preparation.
21. T. C. Johns *et al*., *Clim. Dyn.* **20**, 583 (2003).
22. B. D. Santer *et al*., *Science* **301**, 479 (2003).
23. J. Lean, J. Beer, R. Bradley, *Geophys. Res. Lett.* **22**, 3195 (1995).
24. M. Sato, J. E. Hansen, M. P. McCormick, J. Pollack, *J. Geophys. Res.* **98**, 22987 (1993).
25. J. Lean, *Geophys. Res. Lett.* **27**, 2425 (2000).
26. N. G. Andronova, E. V. Rozanov, F. Yang, M. E. Schlesinger, G. L. Stenchikov, *J. Geophys. Res.* **104**, 16807 (1999).
27. G. A. Meehl, W. M. Washington, T. M. L. Wigley, J. M. Arblaster, A. Dai, *J. Clim.* **16**, 426 (2003).
28. D. V. Hoyt, K. H. Schatten, *J. Geophys. Res.* **98**, 18895 (1993).
29. C. Ammann, G. A. Meehl, W. M. Washington, C. Zender, *Geophys. Res. Lett.* **30**, 1657 (2003).

30. We acknowledge the assistance of the many scientists who developed the observational data sets and the climate models used in this study. Constructive comments from a number of reviewers helped to improve this manuscript. Supported by a Discovery grant from the Australian Research Council (K.B.); the UK Department for Environment, Food and Rural Affairs under contract PECD 7/12/37 (P.A.S.); and NSF and the Office of Biological and Environmental Research, U.S. Department of Energy (J.M.A., G.A.M.).

Supporting Online Material

www.sciencemag.org/cgi/content/full/302/5648/1200/DC1
Materials and Methods
References

14 July 2003; accepted 29 September 2003

Ice Core Evidence for Antarctic Sea Ice Decline Since the 1950s

Mark A. J. Curran,[1]* Tas D. van Ommen,[1] Vin I. Morgan,[1] Katrina L. Phillips,[2] Anne S. Palmer[2]

The instrumental record of Antarctic sea ice in recent decades does not reveal a clear signature of warming despite observational evidence from coastal Antarctica. Here we report a significant correlation ($P < 0.002$) between methanesulphonic acid (MSA) concentrations from a Law Dome ice core and 22 years of satellite-derived sea ice extent (SIE) for the 80°E to 140°E sector. Applying this instrumental calibration to longer term MSA data (1841 to 1995 A.D.) suggests that there has been a 20% decline in SIE since about 1950. The decline is not uniform, showing large cyclical variations, with periods of about 11 years, that confuse trend detection over the relatively short satellite era.

Evidence from observations covering the past ~40 years indicates that parts of coastal Antarctica are warming (*1*, *2*), yet there has been a lack of supporting evidence (*2–5*) from a key warming indicator (*6*), namely sea ice. This is primarily due to high regional variability in sea ice coverage (*3*) and the absence of long-term observations. Antarctic sea ice plays a vital role in climate control, ocean-atmosphere heat exchange, ocean circulation, and ecosystem support (*7–10*). Understanding these important roles of sea ice requires an awareness of the variability in sea ice extent (SIE) and the time scales of change.

Little information is available on sea ice trends beyond the last couple of decades, raising several questions: How useful are recent trends in assessing long-term variability? Is Antarctic sea ice in decline? If so, is this decline an effect of global warming? The advent of regular passive microwave information in 1973 has allowed

[1]Department of the Environment and Heritage, Australian Antarctic Division, and Antarctic Climate and Ecosystem Cooperative Research Centre, Private Bag 80, Hobart, Tasmania 7001, Australia. [2]Institute of Antarctic and Southern Ocean Studies, University of Tasmania, Private Bag 77, Hobart, Tasmania 7001, Australia.

To whom correspondence should be addressed. E-mail: mark.curran@utas.edu.au

insight into the extent and character of sea ice surrounding Antarctica, but the lack of data before that time precludes a useful assessment of long-term variability and trend in sea ice coverage and has led to a search for a useful sea ice proxy. One such candidate is methanesulphonic acid (MSA), a product of biological activity in surface ocean water. MSA production is heavily influenced by the presence of sea ice in the Southern Ocean (*11*), and links between ice core MSA records and SIE have been investigated (*12–14*), but so far, none has produced a sea ice proxy record.

Law Dome projects out into the Indian sector of the Southern Ocean (Fig. 1), and at ~66°S is one of the most northerly parts of the entire Antarctic coastline. Consequently, precipitation on Law Dome is susceptible to marine influences and processes, and is sensitive to environmental signals and variability from this region of the ocean. Although Law Dome is a coastal ice core site with high accumulation, the high elevation, low summer temperatures, and lack of katabatic wind ensure good preservation of this ice core record (*15*).

Analyses of ice cores from near Law Dome summit have produced a seasonally resolved MSA record covering the period 1841 to 1995 A.D. (supporting online text). At this site, MSA concentrations peak in January, with essentially zero levels through the winter period (*16*), so we calculated austral summer-centered mean annual concentrations for the 155-year record. MSA is known to exhibit postdepositional movement in ice core records, but because MSA movement is limited at Law Dome (*17*), annual or longer averages used in this study are unaffected by this process.

A 22-year SIE record (1973 to 1994) was obtained from mean monthly passive microwave data compiled by Jacka (*18*). The SIE used in our analysis was calculated as the mean ice edge latitude (or extent) for August, September, and October of each year (1973 to 1994), which we define as SIE_{max}. Annual SIE_{max} was compared with mean annual MSA concentration, centered on the following summer.

The MSA record was compared with SIE_{max} averaged from around the entire Antarctic continent and with individual sectors, with a view to identifying a source region for MSA deposited at Law Dome. Mean annual MSA concentrations are found to be positively correlated with mean annual Antarctic SIE_{max} ($r = 0.48$, $P < 0.02$, $n = 22$), indicating that the Law Dome MSA record captures 23% of the variance in interannual SIE_{max} changes around the entire continent between 1974 and 1995 (fig. S1).

Further comparisons between MSA and SIE_{max} at each 10° sector around the entire Antarctic coast (Fig. 2) show significant correlations in the region surrounding Law Dome (strongest at 100°E, $r = 0.61$, $P < 0.002$). The region of significant correlation extends 30° to either side of Law Dome, and a strong correlation is found between the averaged SIE_{max} from 80°E to 140°E and MSA ($r = 0.60$, $P < 0.002$), explaining 36% of the variance (Fig. 3, inset). The eastern Ross Sea sector (200°E to 250°E) is also found to be significantly correlated ($r = 0.51$, $P < 0.005$) as a result of autocorrelations in SIE (Fig. 2), rather than transport of MSA from this region to Law Dome. The correlation for the 80°E to 140°E sector suggests that MSA production, and subsequent deposition at Law Dome, is related to SIE variations across this region, and the strength of the correlation indicates that the Law Dome MSA record can be used as a sea ice proxy.

In the past, authors have investigated links between Antarctic ice core and aerosol records of biogenic sulfur compounds (MSA and biogenic sulphate) and various other climate records, such as sea ice (*14*, *19*), ocean chlorophyll (*19*), and El Nino–Southern Oscillation (*20*). Although atmospheric sulphate has a number of sources, the exclusive source of MSA is marine phytoplankton, through dimethylsulphide (DMS) oxidation (*21*). The link between ice core MSA and sea ice distribution has been proposed before (*14*), because MSA is an indicator of biological activity, which in turn is assumed to be influenced by sea ice and climate. More specifically, MSA is an indicator of DMS producers, which is a subset of the total phytoplankton population. The link between MSA and sea ice is strengthened when the distribution of these DMS-producing phytoplankton is considered; in the Southern Ocean region, DMS producers are dominated by sea ice algae, the activity of which produces large quantities of DMS in the sea ice zone after sea ice decay (supporting online text). This results in the Southern Ocean DMS flux being dominated by production from the sea ice zone (*11*). Southern Ocean waters seasonally covered by sea ice are a greater source of DMS (hence MSA) than waters without sea ice. Consistent with this, and with our data, it is plausible that the greater the size of this sea ice zone (extent) in a particular year, the more MSA is produced in that year. The detailed mechanism for this relation is expected to be complex, and there are a number of factors compounding why this relation may not hold in other regions (supporting online text).

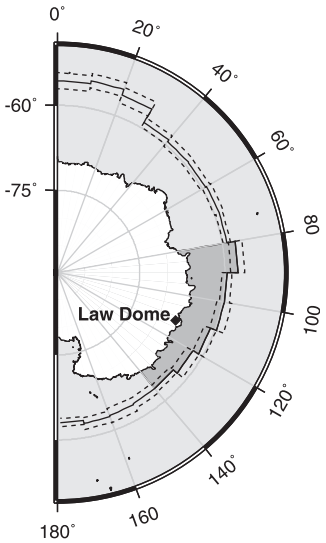

Fig. 1. East Antarctica. The solid line indicates mean annual SIE_{max} in 10° longitude increments (1973 to 1994). The dashed lines are mean ± SD. The heavier shaded region indicates the area of maximum correlation with the Law Dome MSA record.

Coastal Antarctic sulfur aerosol studies provide valuable uniformly sampled high-resolution seasonal information (*19*), but these records are too short to permit interannual comparisons with remotely sensed climate parameters such as sea ice (*19*). In ice core studies, both negative (*12*, *13*) and positive (*14*) sea ice–MSA relations have been found. Negative relations have been reported from both the Arctic (*12*) and the Antarctic Peninsula (*13*). These were due to the dominance of highly localized MSA source regions and a limited fraction of open ocean in summer. The significant positive correlation presented here is supported by an MSA record from a snow-pit study at Newall Glacier, on the western Ross Sea coast of Antarctica (*14*). A positive relation was reported between a monthly time series of sea ice area in the Ross Sea region and an MSA time series (about six samples per year), but the record covered only ~20 years and no conclusions regarding long-term sea ice trends could be made. The Law Dome ice core extends back more than 80,000 years, and further MSA analysis may provide a high-resolution SIE proxy record through the Holocene, as well as information on glacial-interglacial changes, potentially contributing to the debate surrounding the seasonal extent of sea ice during the Last Glacial Maximum (*22*).

The MSA record presented here extends back to 1841 (Fig. 3) and shows considerable decadal-scale variability, with a large decrease in MSA levels since the 1950s. The annual MSA data are shown, and a 3-year running mean is used to reduce interannual noise. The observed MSA variability is independent of other ions and changes in snow

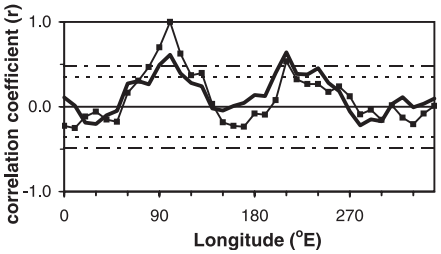

Fig. 2. Correlation coefficients for SIE_{max} at each longitude versus MSA versus SIE_{max} at 100°E (SIE autocorrelation), with the 95% and 99% confidence limits ($n = 22$ years). Solid black line, MSA correlation; thin black line with solid squares, SIE_{max} autocorrelation; dotted line, 95%; dashed line, 99%.

accumulation rate. Although increases in accumulation (and local temperature) are observed for Law Dome between the 1950s and the 1970s (*23*), this pattern is not sustained through to the mid-1990s and cannot explain the MSA changes observed.

The highly significant correlation between the MSA record and SIE is illustrated in Fig. 3, with the overlaid SIE_{max} (1974 to 1995). This agreement allows us to use the MSA record as a proxy to reconstruct SIE, at least in the 80°E to 140°E sector. The relation appears linear for the calibration period (Fig. 3 inset), and a linear response is therefore assumed to apply throughout the record. We interpret variations in the MSA record as changes in SIE in the 80°E to 140°E sector.

Variable-period, high-amplitude quasi-decadal cycles are observed throughout the record. However, in the latter part, when sea ice decline sets in, the cycles become more regular, with an 11-year period. In the available satellite record, there is some evidence of these cycles, although the record is too short to confirm whether they are sustained. Early work by Zwally *et al.* (*24*) alluded to the presence of 10-year cycles in sea ice area, although the researchers came to no definitive conclusion regarding persistent long-term cyclical variations. Later work identified cycles with a period of up to 9 years from a fast-ice record at the South Orkney Islands (*24*), which has been linked to Weddell Sea–pack ice dynamics. These cycles, which could be representative of cycles in SIE in the Weddell Sea region (*25*), mask detection of the long-term trend in the short instrumental sea ice record.

In the 80°E to 140°E region of east Antarctica, the southern boundary of the Antarctic Circumpolar Current (ACC) has been proposed as the factor controlling the northern extent of both sea ice and biological productivity (*7*). Variability in the southern boundary of the ACC may cause the cyclicity observed in our record, but we cannot discount that solar forcing may have a role in the overall control.

A 20-year running mean of the MSA record indicates little overall change between 1841 and about 1950, followed by a steadily declining trend (Fig. 3). We used the linear calibration obtained from the sea ice instrumental data to calculate an inferred change in SIE since the 1950s from 59.3°S to 60.8°S. This change of 1.5° corresponds to a 20% decrease in SIE. This decline is in general agreement with the trend suggested by SIE reconstructions from historical whaling records by de la Mare (*26*) and reports compiled from early Antarctic voyages (*27*). The de la Mare study determined the position of the ice edge between October and April of each year and suggested a 25% decrease in SIE between the 1950s and the 1970s (*26*). Although the quality of the de la Mare data has been challenged (*28*), it remains the only attempt to quantify changes in SIE before satellite data. The confounding effect of the decadal cycles identified here makes a reasonable assessment of the trend over only 2 decades very difficult. For example, if the maximum value of the cycle in the MSA record for the 1950s (Fig. 3) is compared with the minimum value during the 1970s, a decrease in SIE of 2.1° (or a 25% change) is obtained, which agrees with the magnitude of the de la Mare (*26*) findings. The average change, however, is closer to a 12% decrease in SIE between the 1950s and 1970s (20% between the 1950s and 1990s), calculated with our linear technique.

Evidence of sea ice decline is also reported from studies of penguin populations. Adélie penguin populations were shown to be inversely related to winter SIE at Ross Island (*9*), and the populations have been increasing over the past ~40 years. Emperor penguin populations at Dumont d'Urville exhibit a positive relation with SIE, and populations have been decreasing over the past 50 years (*10*).

Sea ice decline is also supported by the small number of Antarctic climate records that extend back to the 1950s, showing a general increase in coastal Antarctic air temperatures (*2*) and a freshening of, and temperature increase in, surface ocean waters (*1*). Modeling studies, based on sea surface temperature anomalies over the past 100 years, suggest annual mean SIE has decreased between 0.7° and 1.2° of latitude (*6*).

The key to the issue of determining sea ice decline is that the length of the record must be considerably longer than the period of the superimposed variability. The reports suggesting that Antarctic sea ice is not in decline, and perhaps has even increased in recent years (*3*–*5*), are based on relatively short satellite records. Misinterpretation can occur when these results are extrapolated and interpreted in terms of an overall trend in climate change, particularly as an indicator of human-induced climate change. For the most part, these reports (*3*–*5*) are consistent with our data: that SIE has increased, or has not changed significantly, between the late 1970s–early 1980s and the mid-1990s (Fig. 3). However, the full MSA record shows that this "apparent" increase is due to the cyclicity within the record. The longer record reveals the underlying long-term decreasing trend.

Although this decreasing trend in SIE is clearly seen in the 80°E to 140°E sector presented here, it is more difficult to distinguish this trend in total Antarctic SIE, which is ultimately more valuable to global climate studies. The natural temporal variability (Fig. 3), combined with regional smoothing effects due to circumpolar propagating and quasi-stationary waves (*29*, *30*), masks detection of the trend in total Antarctic SIE for the short satellite era. Despite this masking, Law Dome MSA remains significantly correlated ($P < 0.02$), with total Antarctic SIE (supporting online text). Because our result is from a single ice core record, other MSA records (both aerosol and ice core) are required to validate this proxy for other sites and ideally to provide records that capture greater variance of the overall Antarctic sea ice variability. Nonetheless, the trend in the sea ice proxy presented here—combined with supporting evidence from whaling records, penguin records, reports from early voyages, records of temperature changes, and climate models—strongly suggest that the total SIE around Antarctica has been in decline since the 1950s.

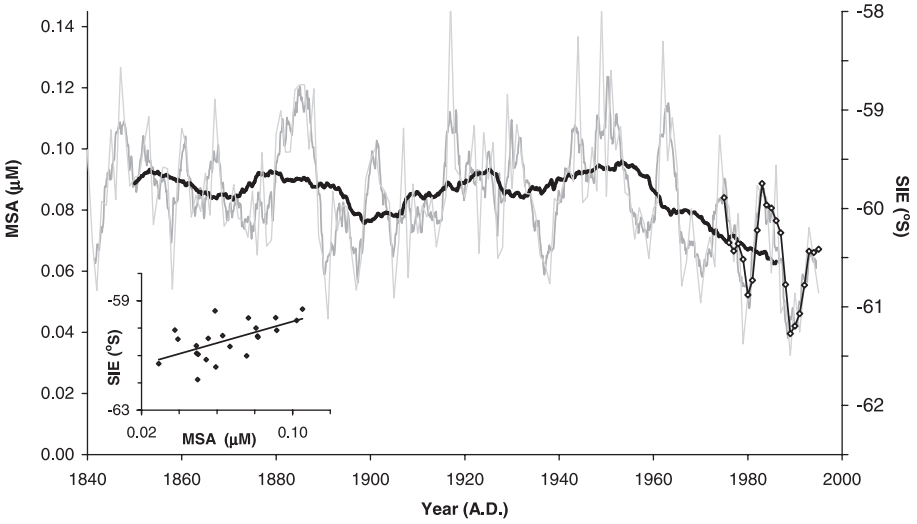

Fig. 3. Law Dome MSA record (1841 to 1995) and SIE_{max} in the 80°E to 140°E sector (1974 to 1995). Faint gray line, MSA annual; thick gray line, MSA 3-year running mean; thick black line, MSA 20-year running mean; black line with open circles, SIE_{max} 3-year running mean. **(Inset)** Correlation of annual MSA with annual SIE_{max} for the overlap period 1974 to 1995 ($P < 0.002$, $n = 22$).

References and Notes

1. S. S. Jacobs, C. F. Giulivi, P. A. Mele, *Science* **297**, 386 (2002).
2. T. H. Jacka, W. F. Budd, *Ann. Glaciol.* **27**, 553 (1998).

3. H. J. Zwally, J. C. Comiso, C. L. Parkinson, D. J. Cavalieri, P. Gloersen, *J. Geophys. Res.* **107**, 9.1 (2002).
4. A. B. Watkins, I. Simmonds, *J. Climate* **13**, 4441 (2000).
5. D. J. Cavalieri, P. Gloersen, C. L. Parkinson, J. C. Comiso, H. J. Zwally, *Science* **278**, 1104 (1997).
6. X. Wu, W. F. Budd, T. H. Jacka, *Ann. Glaciol.* **29**, 61 (1999).
7. S. Nicol *et al.*, *Nature* **406**, 504 (2001).
8. X. Yuan, D. G. Martinson, *J. Clim.* **13**, 1697 (2000).
9. P. R. Wilson *et al.*, *Mar. Ecol. Prog. Ser.* **213**, 301 (2001).
10. C. Barbraud, H. Weimerskirch, *Nature* **411**, 183 (2001).
11. M. A. J. Curran, G. B. Jones, *J. Geophys. Res.* **105**, 20451 (2000).
12. J. O'Dwyer *et al.*, *Geophys. Res. Lett.* **27**, 1159 (2000).
13. E. C. Pasteur, R. Mulvaney, D. A. Peel, E. S. Saltzman, P.-Y. Whung, *Ann. Glaciol.* **21**, 169 (1995).
14. K. A. Welch, P. A. Mayewski, S. I. Whitlow, *Geophys. Res. Lett.* **20**, 443 (1993).
15. V. Morgan *et al.*, *J. Glaciol.* **43**, 3 (1997).
16. M. A. J. Curran, T. D. van Ommen, V. Morgan, *Ann. Glaciol.* **27**, 385 (1998).
17. M. A. J. Curran *et al.*, *Ann. Glaciol.* **35**, 333 (2002).
18. These data are available on the Antarctic Cooperative Research Center and Australian Antarctic Division Climate Data Sets Web site, www.antcrc.utas.edu.au/~jacka/climate.html.
19. A. Minikin *et al.*, *J. Geophys. Res.* **103**, 10975 (2002).
20. M. Legrand, C. Feniet-Saigne, *Geophys. Res. Lett.* **18**, 187 (1991).
21. A. Turnipseed, A. Ravishankara, in *Dimethylsulphide: Oceans, Atmosphere, and Climate*, G. Restelli, G. Angeletti, Eds. (Kluwer Academic, Belgirate, Italy 1993), pp. 185–195.
22. L. K. Armand, A. Leventer, in *Sea Ice: An Introduction to its Physics, Chemistry, Biology, and Geology*, D. N. Thomas, G. S. Dieckmann, Eds. (Blackwell, Oxford, UK, 2003), pp. 333–372.
23. V. I. Morgan, I. D. Goodwin, D. M. Etheridge, C. W. Wookey, *Nature* **354**, 5066 (1991).
24. H. J. Zwally, C. L. Parkinson, J. C. Comiso, *Science* **220**, 1005 (1983).
25. E. J. Murphy, A. Clarke, C. Symon, J. Priddle, *Deep Sea Res. I* **42**, 1045 (1995).
26. W. K. de la Mare, *Nature* **389**, 57 (1997).
27. C. L. Parkinson, *Ann. Glaciol.* **14**, 221 (1990).
28. S. Vaughan, *Polar Record* **36**, 345 (2000).
29. W. B. White, R. G. Peterson, *Nature* **380**, 699 (1996).
30. X. Yuan, D. G. Martinson, *Geophys. Res. Lett.* **28**, 3609 (2001).

Supporting Online Material
www.sciencemag.org/cgi/content/full/302/5648/1203/DC1
SOM Text
Fig. S1
References

11 June 2003; accepted 8 October 2003

Early Allelic Selection in Maize as Revealed by Ancient DNA

Viviane Jaenicke-Després,[1] Ed S. Buckler,[2] Bruce D. Smith,[3] M. Thomas P. Gilbert,[4] Alan Cooper,[4] John Doebley,[5] Svante Pääbo[1]*

Maize was domesticated from teosinte, a wild grass, by ~6300 years ago in Mexico. After initial domestication, early farmers continued to select for advantageous morphological and biochemical traits in this important crop. However, the timing and sequence of character selection are, thus far, known only for morphological features discernible in corn cobs. We have analyzed three genes involved in the control of plant architecture, storage protein synthesis, and starch production from archaeological maize samples from Mexico and the southwestern United States. The results reveal that the alleles typical of contemporary maize were present in Mexican maize by 4400 years ago. However, as recently as 2000 years ago, allelic selection at one of the genes may not yet have been complete.

The wild grass, teosinte (*Zea mays* ssp. *parviglumis*), from which maize (*Zea mays* ssp. *mays*) was domesticated, is endemic to southern and western Mexico (*1*). The earliest undisputed archaeological evidence of domesticated maize is 6250 years old (*2*). However, recent molecular data suggest that domestication could have begun as early as 9000 years ago and that the Balsas River Valley in southern Mexico is the likely geographical origin of domestication (*3*). The early history of character selection in maize is documented in the archaeological record by morphological features discernible in cobs. For example, an increase in the number of rows of kernels and a reduction in glume size have been noted in early maize cobs (*4*). By 5500 years ago, kernel size had also increased (*5*). However, nothing is currently known about when characters not observable from the morphology of cobs, such as plant architecture and starch properties, were selected by early farmers.

Recently, a number of genetic loci associated with phenotypic differences between maize and teosinte have been identified (*6–9*), and three genes involved in such differences have been cloned and relatively well characterized in function (*7*, *9*, *10*). In each of these genes, the allelic diversity in maize compared with teosinte has been shown to be reduced, presumably as a result of selection by early farmers. The first gene, *teosinte branched 1* (*tb1*), carries a maize variant that represses the growth in axillary meristems, leading to the unbranched plant architecture typical of maize. It also contributes to the presence of female cobs on the primary branches in maize rather than male tassels as in teosinte (*11*, *12*). The second gene encodes the prolamin box binding factor (*pbf*), which is involved in the control of expression of seed storage proteins in the kernel (*13–15*), whereas the third gene, *sugary 1* (*su1*), encodes a starch debranching enzyme expressed in kernels (*16*). Together with branching enzymes, this enzyme determines the structure of amylopectin (*16*, *17*). The chain length of amylopectin, as well as the ratio of amylose to amylopectin, is important for the gelatinization properties of starch (*9*) and, thus, affects the textural properties of tortillas (*18*, *19*).

Because DNA in archaeological remains is generally degraded to small sizes (*20*), we identified fragments in each gene that are short enough to allow amplification from ancient corn cobs yet distinguish between the spectrum of gene variants (alleles) found in present-day maize and teosinte (*10*). For *tb1*, the allelic variation in contemporary maize and teosinte is well described (*10*). This allowed us to choose a fragment of 56 base pairs (bp) for which maize carries a single allele, Tb1-M1; this allele has a frequency of 36% in teosinte, where a total of six additional alleles exist. In order to characterize the contemporary variation in *pbf* and *su1*, we sequenced a longer segment of each gene in 66 maize landraces from South, Middle, and North America as well as 23 teosinte parviglumis lines (*10*). The estimated number of alleles segregating in maize is reduced about threefold at *pbf* and *su1* in comparison to teosinte (fig. S1, B and C). At *pbf*, we selected a 25-bp fragment in which the alleles Pbf-M1 and Pbf-M2 are carried in 97% and 3% of maize, whereas the same alleles are carried in 17% and 83% of teosinte, respectively (Fig. 1). At *su1*, we selected a 60-bp fragment in which two major alleles, Su1-M1 and Su1-M2, are carried in maize at a frequency of 30 and 62%, respectively, whereas they both are carried in teosinte at a frequency of about 7% (Fig. 1; table S2) (*10*).

We investigated five maize cobs from the Ocampo Caves in northeastern Mexico (Fig. 2) and six cobs from Tularosa Cave in the Mogollon highlands in New Mexico (*10*).

[1]Max Planck-Institute for Evolutionary Anthropology, Deutscher Platz 6, D-04103 Leipzig, Germany. [2]United States Department of Agriculture/Agricultural Research Service and Department of Genetics, North Carolina State University, Raleigh, NC 27695, USA. [3]Archaeobiology Program, Department of Anthropology, National Museum of Natural History, Smithsonian Institution, Washington, DC 20560, USA. [4]Henry Wellcome Ancient Biomolecules Centre, Department of Zoology, University of Oxford, Oxford OX1 3PS, UK. [5]Laboratory of Genetics, University of Wisconsin, Madison, WI 53706, USA.

*To whom correspondence should be addressed. E-mail: paabo@eva.mpg.de